Current Sensorless Broadband Impedance Measurement Technique for Li-ion Battery Applications

1st Jussi Sihvo
Department of Electrical Engineering
Tampere University
Tampere, Finland
jussi.sihvo@tuni.fi

2nd Daniel-Ioan Stroe
AAU Energy
Aalborg University
Aalborg, Denmark
dis@energy.aau.dk

3rd Tomi Roinila
Department of Electrical Engineering
Tampere University
Tampere, Finland
tomi.roinila@tuni.fi

***Abstract*—Battery impedance is an important parameter for estimation of the battery state-of-charge (SOC) and state-of-health (SOH). However, complexity of the measurement implementation most often prevents wider utilization of the impedance measurement in on-board applications. This paper proposes a current sensorless broadband battery impedance measurement method. In the proposed method, the current required for the impedance calculations is estimated based on the voltage measurements and the equivalent circuit resistance with additional circuit inductance compensation. With the proposed methods, the battery impedance can be obtained accurately with a simple measurement circuit without current measurements. Thus, the method significantly reduces the hardware requirements of the measurements.**

***Index Terms*—component, formatting, style, styling, insert**

I. Introduction

Li-ion batteries have been become an important energy storage technology in the energy and transportation sectors. Li-ion batteries are most often equipped with a battery-management-system (BMS). The BMS monitors the battery voltages, current and temperature which are further used to estimate the battery state-of-charge (SOC) and state-of-health (SOH). The accurate estimation of these parameters is playing a key role in maximizing the safety, efficiency and lifetime of the Li-ion battery systems. [1]

It is widely recognized that the battery internal impedance can be used to improve the estimation accuracy of the SOC and the SOH [2], [3]. In the laboratory conditions, the battery impedance is typically obtained by the electrochemical-impedance-spectroscopy (EIS) measurement technique. The EIS utilizes sinusoidal measurement signal which is injected to the battery current in order to create a voltage response to the battery terminals [4]. Despite being effective method, the utilization of the EIS have so far been very limited in practical battery applications [5]. This is mostly due to the slowness and high complexity of the EIS measurements. In general, the extensive hardware and software requirements of the impedance measurement circuit, measurement probes and data acquisition makes it challenging to make the impedance measurements practically and economically feasible. Thus, new innovations are required to allow feasible integration of the impedance measurements into battery applications.

Recently, pseudo-random-sequence (PRS) signals have been shown to provide rapid impedance measurements with reduced hardware requirements over the EIS [6]. The PRS signals have typically two or three signal levels which allows to use extremely simple measurement circuit, such as, a switch-resistor circuit. In such a simple circuit, the battery current is defined by the battery terminal voltage and the equivalent resistance of the circuit. This allows to estimate the battery current and to exclude the current sensor from the measurement setup which significantly reduces the hardware and software complexity of the measurements. By default, the obtained current estimate is ideal and it does not take the parasitic effect of the circuit inductance into account. The effect of inductance is, however, possible to be taken into account by applying preliminary calibration measurements for the circuit. This allows to obtain consistent results especially at high-frequency region of the impedance where the inductance has a dictating effect.

This paper proposes a current estimation method for Li-ion battery impedance measurements carried out by using three-level direct-synthesis-ternary (DST) sequence measurement signal. In the method, the current is estimated by the measurement circuit equivalent resistance and the battery voltage measurements with additional inductance compensation provided. The methods are validated to results obtained with a current sensor for various types of battery cells and it is shown that the proposed methods produces accurate results. The presented methods can invalidate the need of current sensors which significantly reduces the complexity of the impedance measurements, making the measurements more feasible for practical battery applications.

The rest of the paper is organized as follows: The impedance measurements and the applied measurement circuit are presented in Section II. The proposed current estimation method along with the applied compensation of the circuit inductance, and their experimental validation are presented in Sections III and IV, respectively. At last, the conclusions are drawn in Section V.

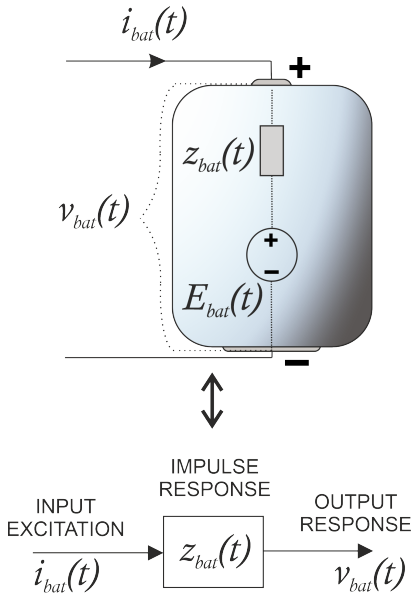

Fig. 1. Correlation of the battery impedance model and the impulse response between the battery current and voltage

II. Battery Impedance Measurements with the PRS Methods

Battery impedance is an intrinsic property of a battery cell describing losses taking place when a current is applied to the cell as illustrated in Fig. 1. Thus, the impedance can be treated as an impulse response $z_{\text{bat}}(t)$ which creates an output response to battery voltage $v_{\text{bat}}(t)$ when applying a suitable input excitation to the battery current $i_{\text{bat}}(t)$. The impedance can be further accessed in the frequency domain by applying Fourier-transform and Ohm's law as given in (1).

$$Z_{\text{bat}}(j\omega) = \frac{V_{\text{bat}}(j\omega)}{I_{\text{bat}}(j\omega)}. \tag{1}$$

Fig. 2 visualises a conceptual Li-ion battery impedance plot in a flipped complex-plane. Usually, the impedance has a non-linear semicircle-shaped form and very low magnitude. In addition, it provides useful information for different state-estimation purposes at relatively wide range of frequencies [7]. In order to obtain tolerable accuracy, speed and overall

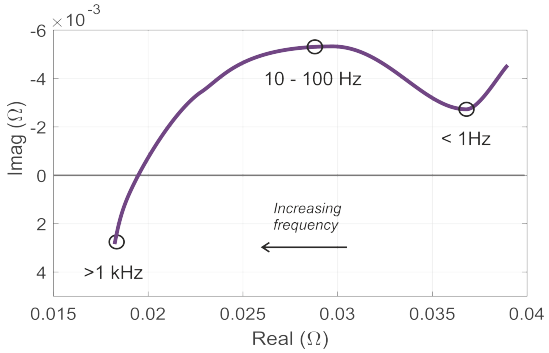

Fig. 2. Conceptual battery impedance plot in a flipped complex-plane

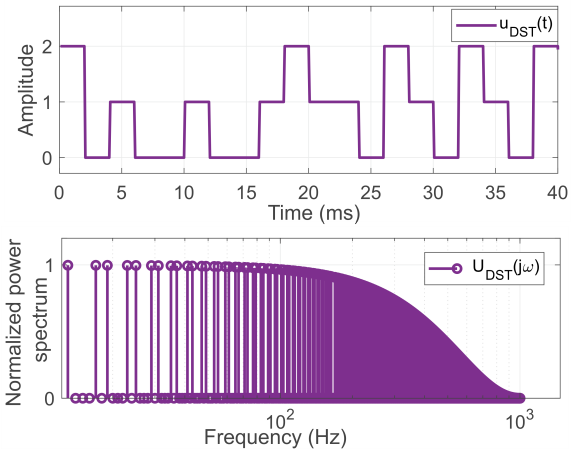

Fig. 3. Sample of a DST sequence in the time- and frequency domains

implementation complexity for measurements with such specifications, the selection of the excitation signal plays a key role. For example, the traditional single-sine EIS is highly accurate but a very complex and slow method. These limitations can be overcome, for example, by pseudo-random-sequence (PRS) signals to make the measurements more feasible in practical applications. The PRS signals are broadband signals that consists only a few signal levels [8], [9]. In particular, recent studies have demonstrated the use of a three-level direct-synthesis-ternary (DST) sequence to work well for measurements of a non-linear system, such as, batteries [6].

Fig. 3 shows a sample of a DST sequence in time- and frequency domains. The DST sequence has frequency harmonics that has zero energy which prevents the effect of nonlinear distortion from contributing to the measurements [9]. In addition, the non-zero harmonics have consistent power spectrum. The three-level form of the DST sequence can be excited to battery current with a simple switch-resistor circuit shown in Fig. 4. The three symmetrical states of the DST sequence can be created by two identical parallel-connected switch-resistor pairs with resistor values $R_{1\text{-}2}$ and switches $S_{1\text{-}2}$ with parasitic resistances $r_{\text{S1-2}}$. During the state "0", both of the switches S1 and S2 are open, making no current flowing in the circuit. During state "1", S1 is closed and S2 open. During state "2", both of the switches are closed which yields to a maximum current drawn from the battery during measurements.

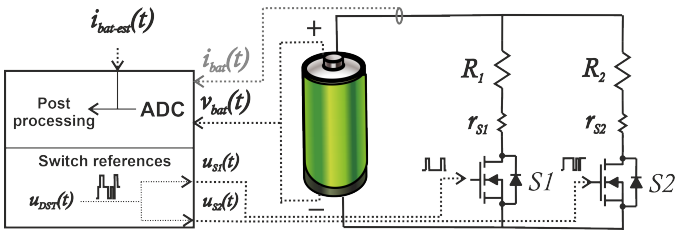

Fig. 4. Switch-resistor measurement circuit and setup for the DST sequence impedance measurements

III. Proposed Current Estimation Method

In the measurement circuit shown in Fig. 4, the current of the circuit is predefined by its total resistance at each DST state, and the battery voltage. This makes it possible for the current to be estimated instead of measured. The measurement circuit's two switch-resistor branches have equivalent resistance $R = R_1 + r_{S1} = R_2 + r_{S2}$. The total resistance of the circuit changes according to R and the DST sequence $u_{DST}(t)$ which, together with the battery voltage, defines the estimated ideal battery current as given in (2).

$$i_{\text{est-ideal}}(t) = \frac{v_{\text{bat}}(t)u_{\text{DST}}(t)}{R}. \tag{2}$$

In reality, the measurement circuit has intrinsic inductance which is mostly caused by the switching characteristics of MOSFETs and circuit wirings. It tends to delay the circuit current which, if not compensated, makes the current-estimated impedance to drift from the reference impedance especially at high frequencies. The measurement circuit of Fig. 4 can be approximated as a series LR circuit. In such a circuit, by applying a step current, the instantaneous current $i$inst(t) is defined as given in (3), where $i_{\text{steady-state}}(t)$ is the steady-state current, R is the circuit resistance and L the inductance.

$$i_{\text{inst}}(t) = i_{\text{steady-state}}(1 - e^{-Rt/L}) \tag{3}$$

As the L is parasitic feature of the measurement circuit, it is difficult to be quantified without prior knowledge of the circuit electrical behavior. Thus, preliminary calibration can be performed for the measurement circuit with external current measurements, and to obtain L from the current rise time with the use of the LR circuit time constant R/L. However, this method can have practical limitations as it requires high sampling rate for the current measurements. Moreover, when lower sampling rate is applied for the voltage measurements in the actual impedance measurements, the term $(1-e^{-Rt/L})$ is replaced by a nonlinearly decaying term, making the circuit no longer linear.

In this paper, instead of obtaining a value for L, the effect of inductance is compensated by using a compensation factor $C_{\text{comp}}(t)$ obtained by preliminary current measurements applied to the circuit. The objective is to add correction term to $u_{\text{DST}}(t)$ in (2) in order to make the estimated, inductance compensated current $i_{\text{est-comp}}(t)$ to match the measured current $i_{\text{meas}}(t)$ as given in (4). Furthermore, the equation can be rearranged in order to obtain $C_{\text{comp}}(t)$ as given in (5).

$$i_{\text{est-comp}}(t) = i_{\text{meas}}(t) = \frac{v_{\text{bat}}(t)(u_{\text{DST}}(t) + C_{\text{comp}}(t))}{R} \tag{4}$$

$$C_{\text{comp}}(t) = \frac{i_{\text{meas}}(t)R}{v_{\text{bat}}(t)} - u_{\text{DST}}(t) \tag{5}$$

The obtained $C_{\text{comp}}(t)$ is a measureless correction term which is characteristic for the measurement circuit regardless of the measured cell. However, specific measurement parameters needs to be kept fixed, such as, the sampling rate and generation frequency of the DST sequence. In addition, high variations in the temperature of the measurement circuit can have effect on the circuit inductance. Therefore, $C_{\text{comp}}(t)$ can be obtained from the calibration measurements at different operating conditions in order to maintain the consistency of the measurements in applications where the measurement conditions are likely to change.

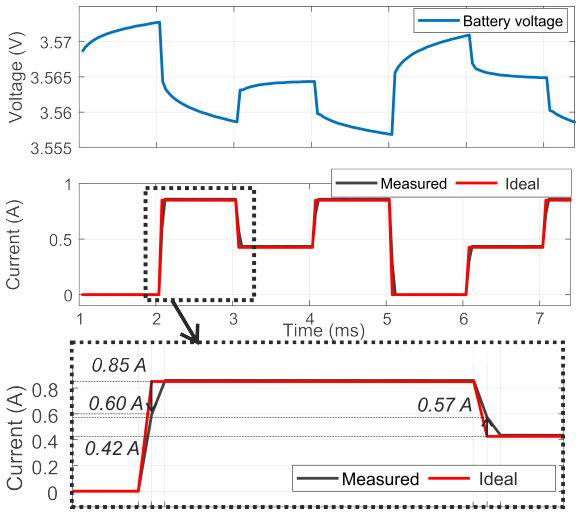

Fig. 5. Sample of the battery voltage and current profiles of the low-frequency sub-band calibration measurements

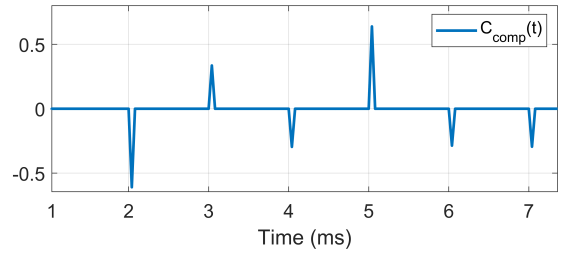

Fig. 6. Sample of the compensation term of the low-frequency sub-band

IV. Experiments

The proposed methods are demonstrated in the experiments by utilizing the setup in Fig. 4. The switch references are created by a MCU in which high-precision ADCs are used for voltage measurements. For inductance compensation and validation, additional current probe is used to measure the battery current. The DST sequence of length 2082 is used for the measurements. The measurements are carried out by using two different sub-bands according to [10]. The DST sequence for the low-frequency sub-band is generated at 1kHz while the high-frequency sub-band is generated at 5kHz. Both of the sequences are sampled at 25kHz. The eventual unition of the sub-bands results in a total bandwidth of 1Hz - 3kHz for the measurements. S1 and S2 are MOSFET switches with $r_{\text{S1-2}} = 0.65\Omega$, and the resistors $R_{\text{1-2}} = 7.7\Omega$. These yield to a total value of $R = 8.35\Omega$ for both switch-resistor branches. A fixed temperature of 25°C is maintained throughout the experiments.

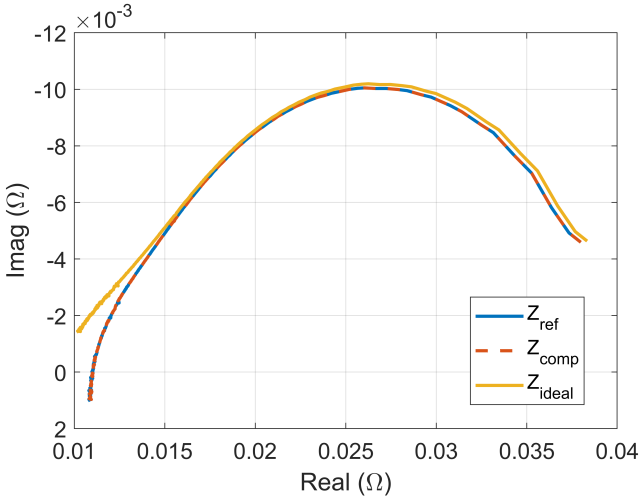

Fig. 7. Impedances of Cell 1 (test cell)

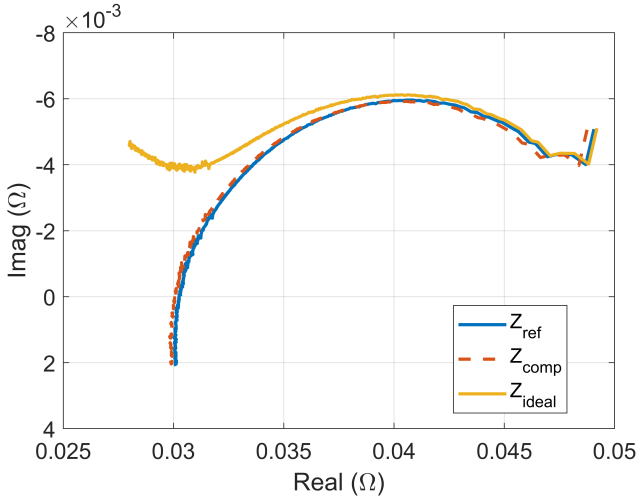

Fig. 9. Impedances of Cell 3

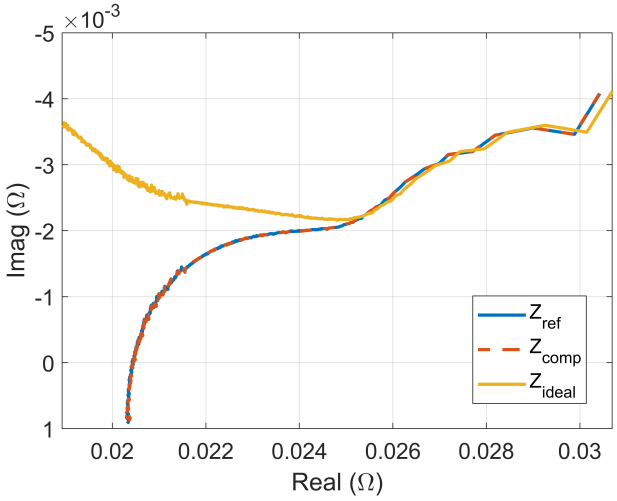

Fig. 8. Impedances of Cell 2

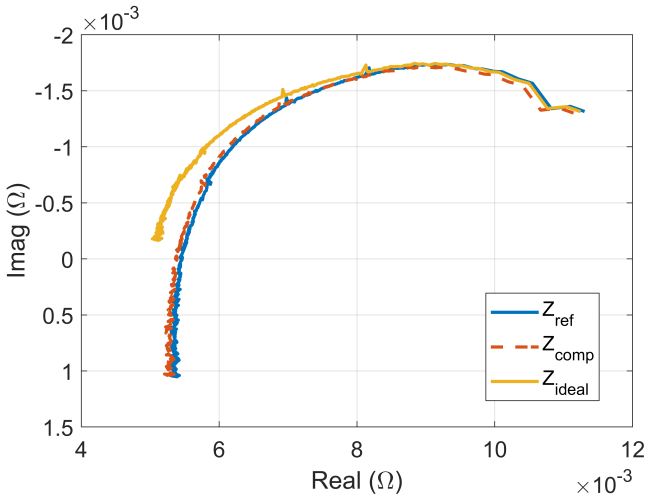

Fig. 10. Impedances of Cell 4

A. *Compensation of the circuit inductance*

To obtain the inductance compensation term $C_{\text{comp}}(t)$ for the experiments, calibration measurements are applied to the measurement circuit by using NMC Li-ion battery cell with a terminal voltage of 3.58V in prior to the calibration. As the measurements are carried out by using two sub-bands, separate compensation terms $C_{\text{comp-low}}(t)$ and $C_{\text{comp-high}}(t)$ needs to be defined for the low- and high-frequency sub-bands, respectively.

Fig. 5 shows a sample of the low-frequency sub-band battery voltage and current along with the ideal current obtained from (2). With the used measurement data acquisition parameters, the effect of inductance is present in the measurements only at the first sample of each state transition. This can also be seen from Fig. 6 which shows a sample of the low-frequency sub-band $C_{\text{comp}}(t)$ obtained from (5). Since the sampling frequency is the same for both sub-bands, the effect is similar also on the high-frequency sub-band. Noteworthy, the magnitude of the non-zero values in $C_{\text{comp}}(t)$ has only 4 different depending on the state transitions in u_{DST} two of which have the same magnitude but opposite signs. In other words, the relative effect of the inductance is same at every transition which allow to create $C_{\text{comp}}(t)$ even from a single current step response.

B. *Impedance measurements*

The proposed methods are validated on carrying out the impedance measurements for four different battery cells denoted as Cell 1 - Cell 4. Cell 1 is the test cell used to obtain the two compensation terms for inductance compensation. For measurements on each cell, the same inductance compensation terms obtained in Section IV-A are used for validation. Cells 1 - 2 are NMC cells and Cells 3 - 4 are Lithium-iron-phosphate (LFP) cells. In addition, cell 4 is a cylindrical 26650 while the rest are cylindrical 18650 cells.

Figs. 7 - 10 shows the impedances of the four cells in the complex-plane with a flipped imaginary axis. In all of the

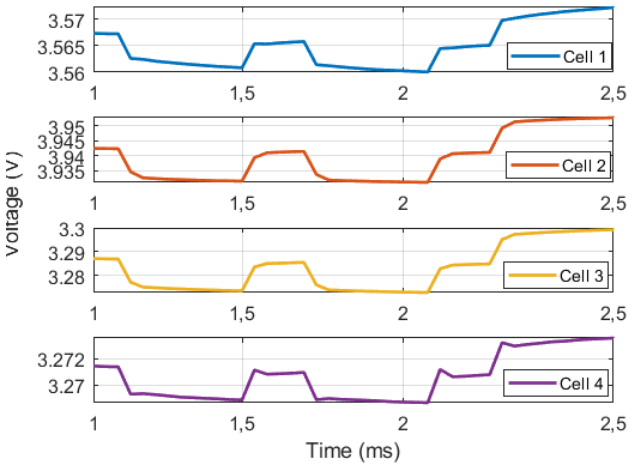

Fig. 11. Samples of the voltage profiles of the measured cells from high-frequency sub-band measurements

figures, Z_{ref} is the reference impedance obtained with current measurements, Z_{comp} is inductance compensated impedance where the current is estimated from (4), and Z_{ideal} is the estimated current obtained from (2) without inductance compensation applied. In Fig. 7, Z_{ref} and Z_{comp} are overlapping because it is the cell used for obtaining $C_{\text{comp}}(t)$. Highly accurate results are also obtained for the Cell 2 impedances as can be seen from Fig. 8. In Figs. 9 - 10, the inductance compensated impedances matches the reference accurately with only small offset realized towards real-axis. This is most likely caused by the mutual effect of the measurement circuit resistor tolerance and $C_{\text{comp}}(t)$. To conclude, a single calibration measurements applied for inductance compensation works well regardless of the measured battery cell.

In the figures, Z_{ideal} deviates from the reference increasingly towards higher frequencies because of the uncompensated inductance of the current estimate. However, the size of the deviation is highly different which is caused by the measured voltage profiles of the cells at the time of the u_{DST} state transition. Fig. 11 shows samples of measured voltage profiles from the high-frequency sub-band measurements. At the time of each state transit, the voltage of Cells 1 and 4 immediately rises/decays to the steady-state voltage of each state with Cell 4 even temporarily peaking above the steady-state. For Cells 2-3, the rising/decaying is slower, yielding to a more capacitive behavior of the cells. This can also be seen from the corresponding impedance plots. While theoretically the voltage describes the dynamic properties of the battery completely, the measured cell voltages includes the effect of the circuit inductance. Therefore, it is useful to include the same effect on the current estimate in order to get valid results for performance testing and state-estimation purposes.

V. Conclusion

This paper demonstrates a current estimation method for Li-ion battery broadband impedance measurements carried out with DST excitation signal. The results show that the impedance can be accurately obtained with the proposed current-estimation methods. The high-frequency part can be accurately corrected by applying the proposed inductance compensation methods. With the proposed methods, the complexity and requirements of the impedance measurements can be significantly reduced, making the measurements more feasible to be used on-board for the SOC and the SOH estimation algorithms in practical battery applications.

References

[1] Y. Wu, *Lithium-Ion Batteries Fundamentals and Applications*. CRC Press, 2015.

[2] Q. Zhang *et al.*, "Electrochemical impedance spectroscopy based state-of-health estimation for lithium-ion battery considering temperature and state-of-charge effect," *IEEE Transactions on Transportation Electrification*, vol. 8, no. 4, pp. 4633–4645, 2022.

[3] U. Westerhoff *et al.*, ""electrochemical impedance spectroscopy based estimation of the state of charge of lithium-ion batteries," journal of energy storage, vol. 8, pp. 244-256,," 2016.

[4] E. Karden, S. Buller, and R. W. De Doncker, "A method for measurement and interpretation of impedance spectra for industrial batteries," *Journal of Power Sources*, vol. 85, no. 1, pp. 72–78, 2000.

[5] N. Meddings *et al.*, "Application of electrochemical impedance spectroscopy to commercial li-ion cells: A review," *Journal of Power Sources*, vol. 480, p. 228742, 2020.

[6] J. Sihvo *et al.*, "Soh analysis of li-ion battery based on ecm parameters and broadband impedance measurements, iecon 2020 the 46th annual conference of the ieee industrial electronics society, pp. 1923-1928,," 2020.

[7] C. Pastor-Fernández *et al.*, "A comparison between electrochemical impedance spectroscopy and incremental capacity-differential voltage as li-ion diagnostic techniques to identify and quantify the effects of degradation modes within battery management systems," *Journal of Power Sources*, vol. 360, pp. 301–318, 2017.

[8] K. Godfrey, H. Barker, and A. Tucker, ""comparison of perturbation signals for linear system identification in the frequency domain," iee proceedings-control theory and applications, vol. 146, no. 6, pp. 535-548,," 1999.

[9] A. H. Tan, "Direct synthesis of pseudo-random ternary perturbation signals with harmonic multiples of two and three suppressed," *Automatica*, vol. 49, no. 10, pp. 2975–2981, 2013.

[10] J. Sihvo, T. Roinila, and D.-I. Stroe, "Broadband impedance measurement of lithium-ion battery in the presence of nonlinear distortions," *Energies*, vol. 13, no. 10, pp. 1–15, 2020.